ACS Photonics

Article

pubs.acs.org/journal/apchd5

$CsPbBr_3$ Perovskite Quantum Dot Vertical Cavity Lasers with Low Threshold and High Stability

Chun-Ying Huang,[†,‡,⊥] Chen Zou,[†,⊥] Chenyi Mao,[§] Kathryn L. Corp,[§] Yung-Chi Yao,[¶] Ya-Ju Lee,[¶] Cody W. Schlenker,[§] Alex K. Y. Jen,[§,∥] and Lih Y. Lin*[,†]

[†]Department of Electrical Engineering, [§]Department of Chemistry, and [∥]Department of Material Science and Engineering, University of Washington, Seattle, Washington 98195, United States

[‡]Department of Applied Materials and Optoelectronic Engineering, National Chi Nan University, NanTou 54561, Taiwan

[¶]Institute of Electro-Optical Science and Technology, National Taiwan Normal University, Taipei 116, Taiwan

Supporting Information

ABSTRACT: All-inorganic cesium lead bromide ($CsPbBr_3$) perovskite quantum dots (QDs) have recently emerged as highly promising solution-processed materials for next-generation light-emitting applications. They combine the advantages of QD and perovskite materials, which makes them an attractive platform for achieving high optical gain with high stability. Here, we report an ultralow lasing threshold (0.39 $\mu J/cm^2$) from a hybrid vertical cavity surface emitting laser (VCSEL) structure consisting of a $CsPbBr_3$ QD thin film and two highly reflective distributed Bragg reflectors (DBRs). Temperature dependence of the lasing threshold and long-term stability of the device were also characterized. Notably, the $CsPbBr_3$ QDs provide superior stability and enable stable device operation over 5 h/1.8×10^7 optical pulse excitations under ambient conditions. This work demonstrates the significant potential of $CsPbBr_3$ perovskite QD VCSELs for highly reliable lasers, capable of operating in the short-pulse (femtosecond) and quasi-continuous-wave (nanosecond) regimes.

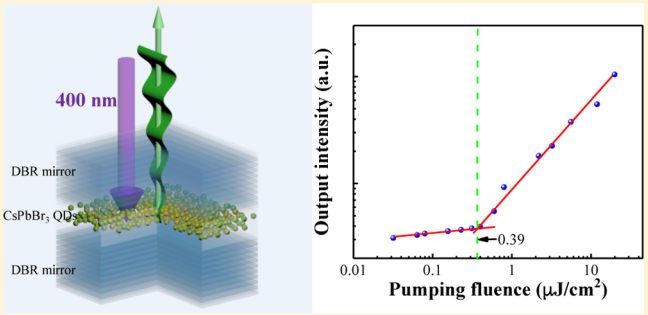

KEYWORDS: *perovskite, $CsPbBr_3$ quantum dots, vertical cavity surface emitting lasers, lasing, threshold, stability, DBR, amplified spontaneous emission (ASE)*

Over the past few years, solution-processed organic–inorganic halide perovskite materials such as $APbX_3$ (A = methylammonium (MA) or formamidinium (FA); X = Cl, Br, or I) have emerged as a compelling newcomer among photonic materials, particularly for photodetection and photovoltaic applications.[1−5] These materials exhibit high carrier mobility,[6] sharp optical absorption edges, and high photovoltaic efficiency,[7] as well as an unusual defect tolerance.[8] The unique optoelectronic properties have led to record certified research solar cell power conversion efficiencies as high as 22.1%.[9] More recently, the application of perovskites as light-emitting materials[10−13] has given rise to new prospects for light-emitting diodes (LEDs),[14,15] amplified spontaneous emissions (ASE),[16−18] and lasing.[19−25] However, a major concern for these perovskite materials is their poor stability upon exposure to moisture, thermal stress, and light.[26,27] This remains an impediment for realizing practical and commercial perovskite-based optoelectronic devices. As a result, many research efforts have been devoted to improving the stability of perovskite devices.[28,29]

To address the aforementioned issues, an alternate approach is to abandon the organic cation by replacing MA or FA with cesium (Cs). This kind of cation engineering, yielding a perovskite-like thin-film structure, has been employed for both LEDs and lasers.[30−35] At the same time, quantum dot (QD) structures with high photoluminescence quantum yield (PLQY) resulting from quantum confinement effects[31,36−38] have been incorporated into light-emitting devices to enhance their efficiencies. The quantization of their electron energy levels also implies narrow emission line widths and broad wavelength tunability. To integrate high stability with the merits of quantum confinement, all-inorganic $CsPbBr_3$ QDs and nanowires have been synthesized and employed for ASE and lasing.[16,18,31,39] However, these studies focused chiefly on the gain media without integrating external resonant cavities. Most recently, a $CsPbBr_3$ vertical cavity laser with 9 $\mu J/cm^2$ lasing threshold was reported.[40] A well-designed resonant cavity is a critical step to achieve lasing in a single-mode Gaussian beam with high directionality, which is important for optoelectronic integrated circuits, especially for optical communication applications.

In the last three decades there have been significant advances in vertical cavity surface emitting lasers (VCSELs), which have attracted wide attention owing to their low lasing threshold, low

Received: May 24, 2017
Published: August 7, 2017

DOI: 10.1021/acsphotonics.7b00520
ACS Photonics 2017, 4, 2281−2289

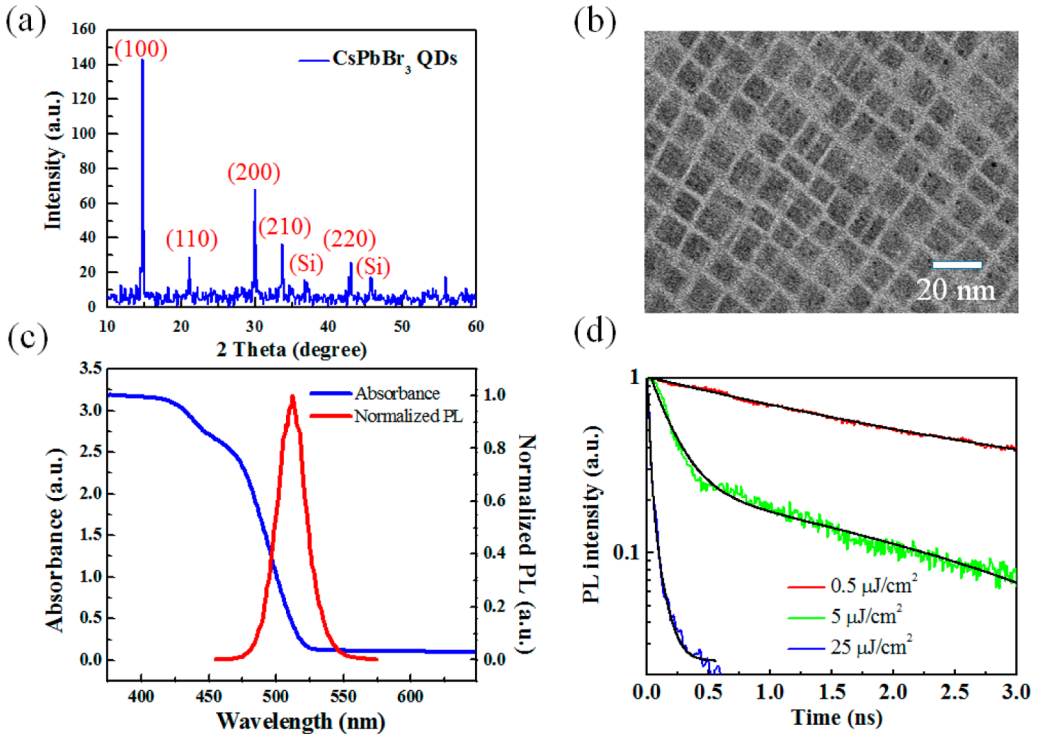

Figure 1. (a) XRD pattern of the $CsPbBr_3$ QD film. (b) TEM image of monodisperse $CsPbBr_3$ QDs. (c) UV−vis absorption and photoluminescence spectra of $CsPbBr_3$ QDs. (d) Time-resolved photoluminescence measurements from the $CsPbBr_3$ QD film under different pump intensities.

beam divergence, circular beam profile, and simplified two-dimensional array architecture compared to edge-emitting lasers.[41−43] The laser cavity consists of two highly reflective distributed Bragg reflector (DBR) mirrors parallel to each other and a gain medium sandwiched in between for stimulated emissions. Most of the VCSELs that have been demonstrated use quantum well structures as the gain medium layer. More recently, colloidal semiconductor QDs have been applied to VCSELs in the visible wavelength range.[44] Semiconductor QDs can reduce the temperature sensitivity of a lasing threshold compared to quantum wells due to their high, delta-function-like density of states profile. Light in the green-wavelength region (typically 500−550 nm) induces maximum luminous sensation for the human eye and thus has a wide range of applications. However, to achieve VCSELs emitting green wavelengths at room temperature has been a challenge (the so-called green gap).[45] Green lasers in general are produced through frequency-doubling technologies, which typically have low efficiencies.

In this work, we explore a strategy for improving the lasing threshold and stability of perovskite lasers by combining a surface-emitting vertical resonant cavity with $CsPbBr_3$ QDs. The hybrid-integrated perovskite laser, with an emission wavelength of 522 nm, achieved an ultralow lasing threshold of 0.39 $\mu J/cm^2$, which further facilitates long-term stability. The device maintained its performance over 1.8×10^7 optical pulse excitation cycles in a duration of over 5 h.

RESULTS AND DISCUSSION

To characterize the QD perovskite material, we first use X-ray diffraction (XRD) and transmission electron microscopy (TEM). The XRD pattern of $CsPbBr_3$ QDs is shown in Figure 1a. The single peak at 2θ equal to 30.69° can be indexed to the (200) plane of $CsPbBr_3$, which matches well with the cubic perovskite crystal structure of $Pm3m$. Figure 1b shows the TEM image of perovskite QDs. The monodisperse $CsPbBr_3$ QDs have an average diameter of 10 nm, with a cubic shape. The optical properties of the $CsPbBr_3$ QDs are first characterized by measuring the absorption and photoluminescence (PL) spectra. Figure 1c shows typical measured ultraviolet−visible (UV−vis) absorption and PL spectra of the $CsPbBr_3$ QD thin film. The absorption edge and PL peak are located at ∼460 and 510 nm, respectively. The PL spectrum shows a narrow line width with a full width at half-maximum (fwhm) of ∼22 nm. To explore the potential of $CsPbBr_3$ QDs for laser application, we first studied the ASE characteristics from the $CsPbBr_3$ QD thin film by a conventional stripe excitation method reported elsewhere.[18,44] With increasing pump fluence, clear signatures of ASE including a narrower emission band (fwhm = 7 nm) and the threshold behavior with a sudden increase of recorded ASE peak intensity at the pump fluence of 5.6 $\mu J/cm^2$ are readily obtained (see supplementary Figure S3a−c and the corresponding analysis in the Supporting Information). Such a low ASE threshold suggests our material as a promising candidate for lasing with resonant cavities. We also find a red-shift of ∼14 nm for the ASE peak with respect to the PL peak. The ASE peak coincides with the end of the shallow absorption tail (Urbach tail) (see supplementary Figure S3d). This red-shifted ASE may originate from reabsorbance in single-exciton amplification or from biexciton recombination.[18] There are also many other possibilities, such as heating by a pumping source, band gap renormalization, and defect transitions.[12]

Time-resolved PL (TRPL) is a common tool to characterize the excited carrier dynamics in relation to the pumping intensity. Figure 1d exhibits the spectrally integrated PL decay traces from the $CsPbBr_3$ QD thin film under various pump fluences. Under excitation fluence far below the ASE threshold, the PL decay curve follows a single-exponential decay (red trace), consistent with single-exciton recombination. With increasing excitation

DOI: 10.1021/acsphotonics.7b00520
ACS Photonics 2017, 4, 2281−2289

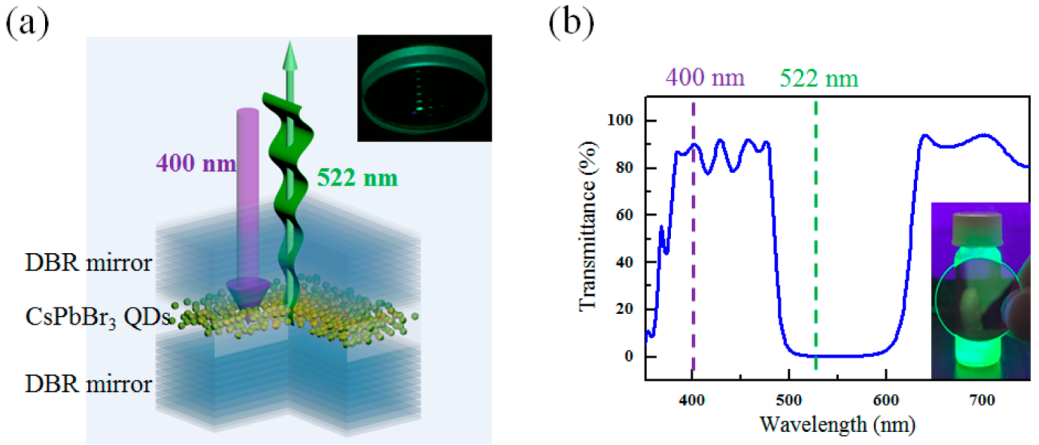

Figure 2. (a) Schematic of the $CsPbBr_3$ QD VCSEL. Inset: Photograph of the device in operation. (b) Transmittance spectrum of the DBR mirror. Inset: Photograph of the mirror in front of an excited $CsPbBr_3$ QD solution. The DBR mirror reflects the green PL while passing the UV excitation light.

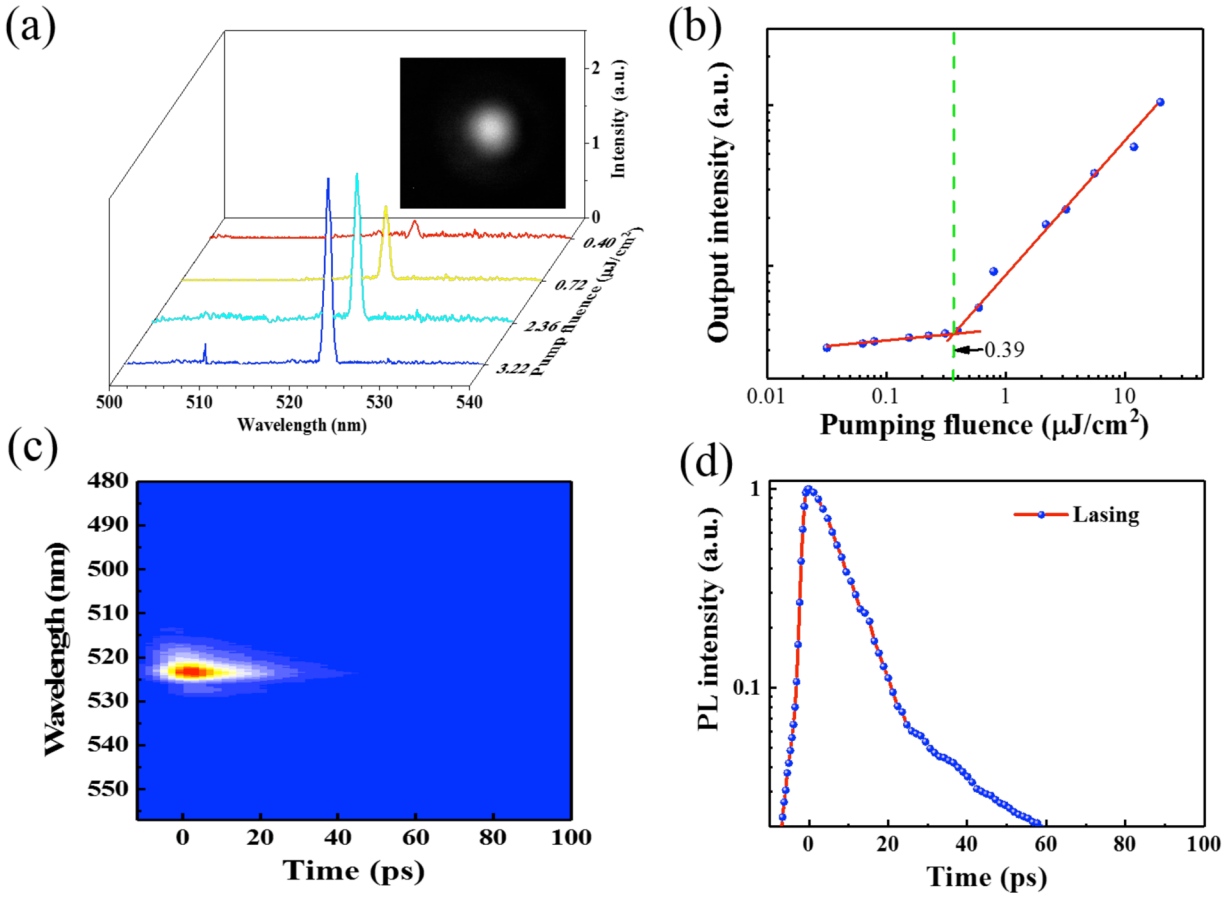

Figure 3. (a) Pump-fluence dependence of the emission spectrum from the $CsPbBr_3$ QD VCSEL. Inset: Far-field image of the emission from a $CsPbBr_3$ QD VCSEL with pumping intensity above the lasing threshold. (b) $L-L$ curve for the $CsPbBr_3$ QD VCSEL, demonstrating lasing with a threshold of 0.39 $\mu J/cm^2$. (c) Spectrogram and (d) PL time response above the lasing threshold. The device was excited at λ = 400 nm with 50 fs laser pulses.

fluence, a fast decay process occurs (green trace), which corresponds to the fast Auger recombination. The lifetime of fast Auger recombination and slow single-exciton recombination is obtained by fitting the PL decay curve with a biexponential decay function. From the best-fitting result, we obtained an Auger recombination lifetime of ~180 ps and a single-exciton recombination lifetime of ~4 ns. Well above the ASE threshold, an ASE lifetime of 30 ps could be estimated from the PL decay (blue trace), again by biexponential fitting, which is comparable to other published results.[18]

After characterizing the material morphology and optical properties of $CsPbBr_3$ QDs, the perovskite thin films were employed as the optical gain medium for laser fabrication. In order to achieve lasing, it is essential to build a resonant cavity with high-reflectivity mirrors (R > 99%). We adopted a vertical cavity design in which the optical gain medium ($CsPbBr_3$ QDs film) is sandwiched between two DBR mirrors parallel to each

DOI: 10.1021/acsphotonics.7b00520
ACS Photonics 2017, 4, 2281−2289

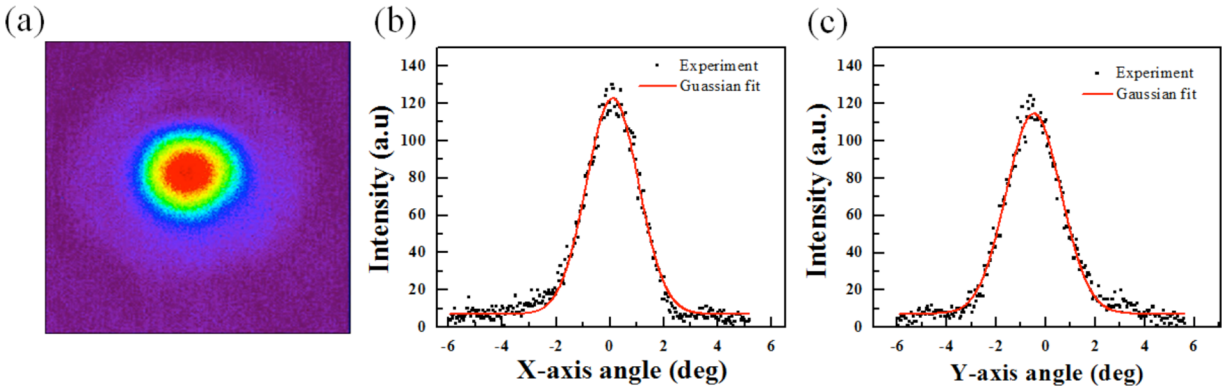

Figure 4. (a) Intensity distribution of the laser emission at 20 cm from the output DBR mirror. (b) Gaussian fitting along the *x*-direction and (c) Gaussian fitting along the *y*-direction. *R*-squared value is ∼0.99.

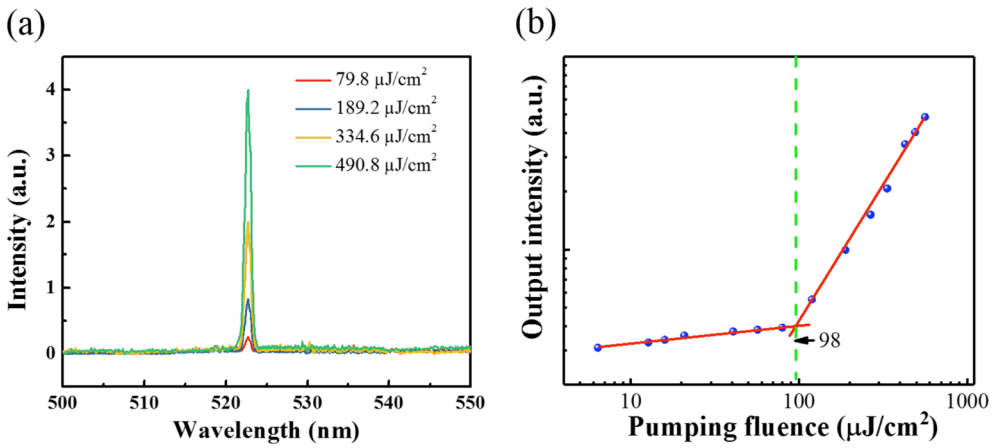

Figure 5. (a) Evolution of the emission spectra with increasing pump fluence for the $CsPbBr_3$ QD VCSEL. (b) *L*−*L* curve for the $CsPbBr_3$ QD VCSEL, showing a lasing threshold at 98 $\mu J/cm^2$. The device was excited at λ = 355 nm with 5 ns laser pulses.

other, as shown in Figure 2a. The inset shows a photograph of the device in operation, emitting green light. To match the peak ASE wavelength of $CsPbBr_3$ QDs (λ = 524 nm), the DBR mirrors need to have a high reflection band covering the green-wavelength range while transmitting the pump wavelength (λ = 400 nm) efficiently ($R \leq 10\%$). A commercially available DBR mirror (FD1M, Thorlabs, Inc.) was found to meet such requirements. As shown in Figure 2b, it has >99% reflectivity around 524 nm and high transparency below 500 nm. The inset of Figure 2b shows a photograph of the DBR mirror in front of the $CsPbBr_3$ QD solution under UV excitation, demonstrating that the mirror reflects the PL while passing the UV light. High-reflection mirrors are critical in VCSELs to compensate the short optical gain length. Typical $CsPbBr_3$ QD solutions have a concentration of ∼10 mg mL^{-1}, resulting in a film thickness below 100 nm by spin-coating at 1000−3000 rpm for 60 s.[34,46] To increase the optical gain length of the VCSEL, we synthesized a $CsPbBr_3$ QD solution with high concentration (55 mg mL^{-1}, see Methods) and the same dispersity and achieved a film thickness of ∼240 nm in the device (see Supporting Information). Combining this thicker film with the high-quality DBR matching the $CsPbBr_3$ QD absorption/emission spectrum is key to achieving perovskite lasers with ultralow lasing thresholds. The overall resonant cavity design results in a lasing wavelength of 522 nm, as illustrated in Figure 2a, and will be discussed next.

The deterministic characteristics of lasing are represented by the dependence of the laser emission spectrum and output optical intensity on the pump fluence. A femtosecond Ti:sapphire laser with optical parametric amplifier output at 400 nm wavelength, 50 fs pulse width, and 1 kHz repetition was first used as the pump source. Figure 3a shows the PL spectra at different pump fluence. The inset shows the image of the $CsPbBr_3$ QD VCSEL output obtained by a CCD camera. Below the lasing threshold, the emission is fully blocked by the DBR mirror, and there is only a broad noisy PL signal detected by the CCD camera. As the pump fluence increases, a narrow peak at λ = 522 nm starts to emerge (fwhm line width $\Delta\lambda$ = 0.9 nm), which red-shifts 12 nm relative to the PL peak. For the VCSEL structure, the cavity modes from vertical cavities determine laser emission wavelengths. We changed the thickness of the perovskite layer and found different emission peak wavelengths from the laser with corresponding variation of the pump threshold (see supplementary Figure S5). An optimized thickness corresponding to the lowest pump threshold is chosen for our device. This results in an emission peak at λ = 522 nm, which is very close to the peak of the gain (ASE) spectrum at λ = 524 nm. Beyond the lasing threshold, the rate of emission through single-exciton or biexciton recombination increases significantly, which greatly benefits stimulated emission over spontaneous recombination.[18] The output intensity versus input pump fluence (*L*−*L* curve) measurement result is shown in Figure 3b. The plot of the *L*−*L* curve exhibits abrupt rising at ∼0.39 $\mu J/cm^2$, further confirming lasing operation beyond this threshold. To gain a deeper insight into our device, we performed PL dynamics measurement on the $CsPbBr_3$ QD VCSEL well

DOI: 10.1021/acsphotonics.7b00520
ACS Photonics 2017, 4, 2281−2289

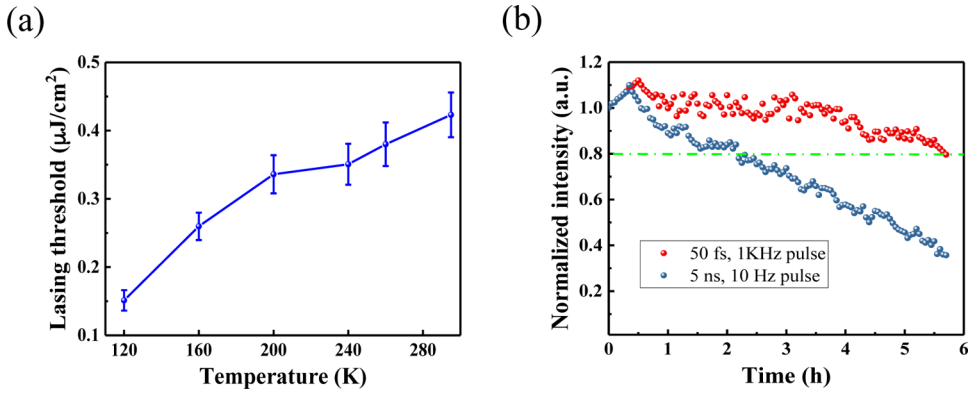

Figure 6. (a) Lasing threshold pump fluence versus temperature for the $CsPbBr_3$ QD VCSEL. (b) Stability characterizations of the device under fs (red) and ns (blue) pulsed excitation with pump fluence set at $1.1P_{th}$. The measurements were performed at room temperature under ambient conditions.

above the lasing threshold at 5 $\mu J/cm^2$. Figure 3c shows the time-resolved spectrogram obtained using a streak camera. The corresponding time-resolved PL intensity is plotted in Figure 3d. The fast decay (~10 ps) at peak wavelength (522 nm) indicates that the emission is mainly through a stimulated process, which provides further confirmation on the lasing operation of the device. The observed decay time is limited primarily by the resolution of the streak camera.

To characterize the laser beam quality, we measured the intensity distribution of the laser beam along the *x*- and *y*-direction at 20 cm from the output of the DBR mirror. Figure 4a shows the measurement result. The corresponding beam profiles along the *x*- and *y*-direction are shown in Figure 4b and c, respectively. The results fit well with a TEM_{00} Gaussian beam (*R*-squared value is ~0.99), demonstrating single-mode operation with high optical beam quality. The fwhm line width for the *x*- and *y*-direction are 2.41° and 2.72°, indicating small beam divergence from our $CsPbBr_3$ QD VCSEL.

For long-term applications, lasers operating under continuous wave (CW) pumping are strongly preferred. In this condition, self-heating under high pumping intensity is a major concern, as it may prevent the device from lasing. This is due to the increased Auger recombination rate when the pump duration becomes longer than the stimulated emission lifetime. In addition to local heating, nonradiative Auger recombination in perovskite QDs may also lead to reduced quantum efficiency and flickered fluorescence emission.[31] In order to probe the potential for CW operation, while still being able to achieve sufficient pump intensity, a quasi-CW pulsed laser with a pulse duration much longer than the Auger lifetime is often utilized.[31,47] We used a nanosecond Nd:YAG laser (355 nm wavelength, 5 ns pulse duration, 10 Hz repetition) to perform such characterizations. The emission spectra from the $CsPbBr_3$ QD VCSEL under different pump fluences are shown in Figure 5a. The output optical intensity versus the pump fluence is shown in Figure 5b. The narrow emission peaks and the kink in the *L*−*L* curve due to transitioning from spontaneous emission to stimulated emission indicate that lasing can still be achieved under such quasi-CW operation. The estimated lasing threshold is 98 $\mu J/cm^2$, which is significantly higher than the 0.39 $\mu J/cm^2$ threshold under fs pulse pumping. This may be attributed to the insulating shell of ligands on the QD surface, which can cause larger thermal load while the device is under CW operation. To address this issue in the future, a possible approach is to perform a ligand exchange to replace long carbon bonds (oleic acid) with short carbon bonds (caprylic acid), which should not affect the dispersion of QD solutions.[48]

To study the temperature dependence of lasing threshold, the *L*−*L* curves of the $CsPbBr_3$ QD VCSEL were recorded under various temperatures from 120 to 295 K. The femtosecond pulsed laser was used as the pump source. Figure 6a shows the experimental results. The lasing threshold decreases steadily with decreasing temperature and ultimately reaches 0.15 $\mu J/cm^2$ at 120 K. This is believed to be due to the combination of increased radiative recombination rate and decreased Auger recombination loss.[49] It is worth noting a difference in temperature dependence between $MAPbX_3$ thin films and $CsPbBr_3$ QDs. The $MAPbX_3$ thin films undergo a phase transition from tetragonal to orthorhombic as the temperature decreases below 160 K, which leads to a sudden increase in the band gap.[50] Consequently, the gain spectrum blue-shifts out of the wavelength range for cavity modes, resulting in laser emission disappearance below 160 K.[19] On the other hand, our $CsPbBr_3$ QD laser can still achieve lasing with decreasing threshold, and the emission peak wavelength changes by a small amount of ~2 nm even when the temperature decreases below 160 K (see supplementary Figure S2).

Long-term reliability is a key issue that needs to be addressed before a laser can be deployed outside a research lab. There have been few studies on stability testing of ASE and lasing in perovskite materials, and the factors leading to long-term device degradation remain unclear.[16,31,35,40,47] It is well-known that all-inorganic perovskite materials (such as $CsPbBr_3$) are more stable than classical inorganic/organic perovskite materials. To evaluate the stability of the $CsPbBr_3$ QD VCSEL under different thermal load, we applied fs and ns excitation pulses to identify the correlation between operation mode (short pulse versus quasi-CW) and lifetime. The devices were optically pumped to $1.1P_{th}$ (P_{th} is the threshold pump fluence) under ambient conditions, and the integrated emission intensities were recorded as a function of time. We defined an 80% lifetime (T_{80}) as the time when the output intensity decreases to 80% of the initial intensity. As shown in Figure 6b, the device under fs pump pulses exhibits higher stability (T_{80} > 5 h/1.8 × 10^7 pump pulses), while the output intensity decreases significantly faster under ns pulse pumping (T_{80} ≈ 2 h). This may be attributed to the decomposition of QDs under higher optical pump power. In other words, higher lasing threshold produces larger joule heating, which can degrade the device performance significantly. Compared to lasers utilizing $MAPbI_3$, where the use of organic material and/or high threshold hinders the device stability, our results reflect the more moderate thermal load, which, together with the utilization of all-inorganic perovskite materials, benefits

DOI: 10.1021/acsphotonics.7b00520
ACS Photonics 2017, 4, 2281−2289

Table 1. Single-Mode Lasing Threshold Comparison between Perovskite Lasers

material	morphology[a]	pump source	threshold (μJ/cm^2)	cavity	published year	ref
$MAPbI_3$	thin film	532 nm/1 ns	0.32	DFB	2016	21
$MAPbI_3$	thin film	515 nm/200 fs	41	DFB	2016	55
		355 nm/0.91 ns	10			
$MAPbI_3$	thin film	532 nm/0.4 ns	~200	PhC	2016	56
$MAPbI_3$	thin film	532 nm/0.27 ns	~69	PhC	2016	51
$MAPbI_3$	thin film	532 nm/0.3 ns	3.8	PhC	2017	57
$MAPbI_3$	thin film	532 nm/0.34 ns	7.6	DBR	2017	47
		532 nm/5 ns	~114			
$CsPbBr_3$	NW	400 nm/150 fs	10	Fabry–Pérot, end facets	2016	35
$CsPbBr_3$	NW	402 nm/150 fs	6.2	Fabry–Pérot, end facets	2016	58
$CsPbCl_3$	thin film	400 nm/150 fs	7.2	microdisk	2017	59
$CsPbBr_3$	NCQD	400 nm/100 fs	11	DBR	2017	40
		400 nm/5 ns	900			
$CsPbBr_3$	NCQD	400 nm/50 fs	0.39	DBR		this work
		355 nm/5 ns	98			

[a]NW stands for nanowire; NCQD stands for nanocrystal quantum dot.

the long-term stability of the lasers. Our results under both fs and quasi-CW ns pulse pumping compare favorably with reported results from literature for perovskite lasers.[35,40,47,51,52]

Table 1 summarizes the device performance comparison in terms of single-mode threshold among perovskite lasers reported in the literature and this work. As there has been a surge in research results on lasing in perovskite materials, we focus the comparison on perovskite lasers with externally defined resonant cavities such as DBR, distributed feedback (DFB), photonic crystal (PhC), and Fabry–Pérot for organic–inorganic lead halide perovskite lasers. Perovskite lasers that utilize these device architectures are more suitable for photonic integrated circuits than platforms that rely on the facets of nanoplatelets and nanowires or perovskite-coated microspheres. Since the number of published reports on all-inorganic perovskite lasers is limited, we also include results from nanowires and patterned microdisks for references. Our device shows a lower lasing threshold than most all-inorganic perovskite lasers and at the same time achieves comparable performance to some organic–inorganic perovskite lasers while exhibiting high stability. Shortly before the initial submission of this work, Wang et al. reported a $CsPbBr_3$ QD VCSEL with a similar structure but a significantly higher lasing threshold (9 μJ/cm^2).[40] The ultralow threshold for double-mode lasing of our device may be attributed to high optical gain of the material (low ASE threshold at 5.6 μJ/cm^2), high transmittance (90%) of the DBR for the pump wavelength, better film quality/surface roughness (see supplementary Figure S1), and especially better matching of the resonant cavity mode with the gain spectrum by optimizing the perovskite film thickness (see supplementary Figure S5). Compared to ref 40, the $CsPbBr_3$ QDs in this work show lower ASE threshold (enhanced optical gain), longer PL lifetime, and smoother film surface, which may be attributed to the better synthesis process. Recently, it has been reported that the solvents used for purifying perovskite QDs and the corresponding washing process are important factors affecting properties of perovskite QDs such as PLQY, PL lifetime, surface roughness, and stability.[16,53,54] In our work, ethyl acetate was adopted to wash perovskite QDs, and octane was used to disperse QDs. These solvents are commonly used in the synthesis process of $CsPbBr_3$ QDs and should be more suitable compared to acetone used in ref 40. The spin-cast method in our fabrication process may also result in higher thin-film quality than the films obtained using drop-casting reported in ref 40. The ultralow threshold lasing performance demonstrates that $CsPbBr_3$ QDs integrated with a high-quality cavity provide a significant step forward toward the next-generation perovskite lasers.

CONCLUSIONS

In summary, we demonstrate a perovskite VCSEL by hybrid integration of $CsPbBr_3$ QDs with DBR mirrors. This approach combines the merit of QDs, namely, high quantum efficiency, with a well-designed resonant cavity through optimized perovskite film thickness and DBR mirrors and achieved an ultralow lasing threshold of 0.39 μJ/cm^2. To the best of our knowledge, this is the lowest reported threshold to date for $CsPbBr_3$ QD lasers and ASE and comparable to the lowest reported threshold of $MAPbX_3$ perovskite lasers. In addition to the ultralow threshold, the utilization of all-inorganic $CsPbBr_3$ QDs resulted in high device stability, and the laser maintained its performance over hours of operation under both fs and quasi-CW ns pulse pumping at ambient conditions. The results demonstrate the strong potential of the proposed approach for ultra-low-threshold, highly stable perovskite lasers toward CW operation in the future.

METHODS

Synthesis of $CsPbBr_3$ Quantum Dots. Cesium carbonate (Cs_2CO_3, 99.9% trace metals basis), lead(II) bromide ($PbBr_2$, 98%), octadecene (ODE, technical grade 90%), oleylamine (OLA, technical grade 70%), and *n*-octane (≥99%) were purchased from Sigma-Aldrich. Oleic acid (OA, technical grade 90%) and ethyl acetate (≥99.5%) were purchased from Alfa Aesar. For the synthesis of Cs-oleate, 0.326 g of Cs_2CO_3 (1 mmol) was loaded into a 100 mL, three-neck flask along with 18 mL of ODE and 1 mL of OA. The mixture was dried for 30 min at 100 °C and then heated under N_2 flow to 150 °C until all Cs_2CO_3 reacted with OA. The clear solution was kept at 150 °C to prevent the solidification of the Cs-oleate solution. For the synthesis of $CsPbBr_3$ QDs, 66.7 mg of $PbBr_2$ (0.18 mmol) was loaded into a 25 mL three-neck flask along with 5 mL of ODE, 1 mL of OLA, and 0.5 mL of OA. The mixture was dried for 10 min at 100 °C and then heated to 150 °C under N_2 until a clear solution was obtained. After the $PbBr_2$ salt had dissolved completely, the temperature was raised to 170 °C and then an as-prepared Cs-oleate solution was swiftly injected. Within seconds,

DOI: 10.1021/acsphotonics.7b00520
ACS Photonics 2017, 4, 2281–2289

the final solution was cooled to room temperature by an ice−water bath. To purify the particles, an excess amount of ethyl acetate was added into the crude solution. The precipitate was collected by centrifugation and redispersed in *n*-octane. The process was repeated several times, and the final product was dispersed in *n*-octane. Before use, the $CsPbBr_3$ QD solution was filtered by a 0.45 μm pore size poly(tetrafluoroethylene) filter to remove precipitates and impurities.

Device Fabrication. Commercially available DBR mirrors (FD1M) with ∼99.5% reflection for 510 nm were purchased from Thorlabs. A set of DBR mirrors were cleaned sequentially with acetone, 2-propanol, and deionized water under sonication for 10 min, respectively. Afterward, the cleaned mirrors were treated with oxygen plasma for 10 min before a spin-coating process. To form highly smooth thin films, a $CsPbBr_3$ QD solution was spin-coated onto one mirror at 1500 rpm for 40 s. To complete the VCSEL structure, the other DBR mirror was bonded to the as-coated mirror with optical epoxy at the periphery. Finally, the device was pressed under a heavy load to minimize the air gap in the cavity during the drying process of optical epoxy for 24 h. The entire process of device fabrication was performed in a Class-100 clean room.

Material Characterization. Powder XRD patterns of $CsPbBr_3$ QDs deposited on a Si substrate were recorded using a Bruker F8 Focus power XRD with monochromatized Cu Kα radiation (λ = 1.5418 Å). TEM and high-resolution TEM were performed on a Tecnai G2 F20 operating at 200 kV. UV−visible absorption spectra of the films were measured with Varian Cary 5000 UV−vis−NIR spectrophotometer. Steady-state photoluminescence emission spectra were acquired using a spectrofluorometer (Fluorolog FL-3, Jobin Yvon Horiba) with a xenon short arc lamp as the light source. For the $CsPbBr_3$ QD thin film, the time-resolved PL measurements were performed using a time-correlated single-photon counting system (FluoTime 100, PicoQuant) while the perovskite thin film was photoexcited by a pump laser source (405 nm, 60 ps, 40 MHz) from PicoQuant.

Device Characterization. A femtosecond Ti:sapphire laser (Coherent, Inc.) with a frequency-doubling external beta barium borate crystal (400 nm, 50 fs, 1 kHz) and a nanosecond Nd:YAG laser (355 nm, 5 ns, 10 Hz) were used as the pump sources. For the steady-state PL and lasing measurement, a home-built micro-PL system was utilized, and the luminescence was recorded by a microspectrometer (OSM-100, Newport) and a spectrometer (iHR550, Horiba Jobin Yvon) equipped with a CCD detector cooled by liquid nitrogen, respectively. For time-resolved spectrogram and PL decay, the emission was collected using a Hamamatsu streak camera (C10910) with the synchroscan attachment (M10911-01). All of the aforementioned measurements were conducted at room temperature. Low-temperature measurements were conducted in a cryostat from Janis Research Inc. The VCSEL device temperature could be adjusted from 120 to 295 K with high precision.

■ ASSOCIATED CONTENT

Supporting Information

The Supporting Information is available free of charge on the ACS Publications website at DOI: 10.1021/acsphotonics.7b00520.

Morphology characterization of $CsPbBr_3$ QD thin films, temperature and active layer thickness dependent performance of $CsPbBr_3$ QD VCSEL devices, ASE characterization, cavity mode analysis, characterization of air gap and optical quality (PDF)

■ AUTHOR INFORMATION

Corresponding Author

*E-mail: lylin@uw.edu.

ORCID

Cody W. Schlenker: 0000-0003-3103-402X

Author Contributions

⊥C.-Y. Huang and C. Zou contributed equally.

Notes

The authors declare no competing financial interest.

■ ACKNOWLEDGMENTS

This work was supported in part by NASA through grant no. NNX13AL60H. C.-Y.H. acknowledges financial support from the Ministry of Science and Technology of Taiwan.

■ REFERENCES

(1) Liu, M.; Johnston, M. B.; Snaith, H. J. Efficient Planar Heterojunction Perovskite Solar Cells by Vapour Deposition. *Nature* **2013**, *501*, 395−398.

(2) Xing, G.; Mathews, N.; Sun, S.; Lim, S. S.; Lam, Y. M.; Grätzel, M.; Mhaisalkar, S.; Sum, T. C. Long-Range Balanced Electron- and Hole-Transport Lengths in Organic-Inorganic $CH_3NH_3PbI_3$. *Science* **2013**, *342*, 344−347.

(3) Green, M. A.; Ho-Baillie, A.; Snaith, H. J. The emergence of perovskite solar cells. *Nat. Photonics* **2014**, *8*, 506−514.

(4) Zuo, F.; Williams, S. T.; Liang, P. W.; Chueh, C. C.; Liao, C. Y.; Jen, A. K. Y. Binary-Metal Perovskites Toward High-Performance Planar-Heterojunction Hybrid Solar Cells. *Adv. Mater.* **2014**, *26*, 6454−6460.

(5) Yang, W. S.; Noh, J. H.; Jeon, N. J.; Kim, Y. C.; Ryu, S.; Seo, J.; Seok, S. I. High-performance Photovoltaic Perovskite Layers Fabricated through Intramolecular Exchange. *Science* **2015**, *348*, 1234−1237.

(6) Ponseca, C. S.; Savenije, T. J.; Abdellah, M.; Zheng, K.; Yartsev, A.; Pascher, T.; Harlang, T.; Chabera, P.; Pullerits, T.; Stepanov, A.; Wolf, J.-P.; Sundström, V. Organometal Halide Perovskite Solar Cell Materials Rationalized: Ultrafast Charge Generation, High and Microsecond-Long Balanced Mobilities, and Slow Recombination. *J. Am. Chem. Soc.* **2014**, *136*, 5189−5192.

(7) De Wolf, S.; Holovsky, J.; Moon, S.-J.; Löper, P.; Niesen, B.; Ledinsky, M.; Haug, F.-J.; Yum, J.-H.; Ballif, C. Organometallic Halide Perovskites: Sharp Optical Absorption Edge and Its Relation to Photovoltaic Performance. *J. Phys. Chem. Lett.* **2014**, *5*, 1035−1039.

(8) Yin, W. J.; Shi, T.; Yan, Y. Unusual Defect Physics in $CH_3NH_3PbI_3$ Perovskite Solar Cell Absorber. *Appl. Phys. Lett.* **2014**, *104*, 063903.

(9) Swarnkar, A.; Marshall, A. R.; Sanehira, E. M.; Chernomordik, B. D.; Moore, D. T.; Christians, J. A.; Chakrabarti, T.; Luther, J. M. Quantum dot−induced phase stabilization of α-CsPbI3 perovskite for high-efficiency photovoltaics. *Science* **2016**, *354*, 92−95.

(10) Stranks, S. D.; Snaith, H. J. Metal-halide Perovskites for Photovoltaic and Light-emitting Devices. *Nat. Nanotechnol.* **2015**, *10*, 391−402.

(11) Colella, S.; Mazzeo, M.; Rizzo, A.; Gigli, G.; Listorti, A. The Bright Side of Perovskites. *J. Phys. Chem. Lett.* **2016**, *7*, 4322−4334.

(12) Veldhuis, S. A.; Boix, P. P.; Yantara, N.; Li, M.; Sum, T. C.; Mathews, N.; Mhaisalkar, S. G. Perovskite Materials for Light-Emitting Diodes and Lasers. *Adv. Mater.* **2016**, *28*, 6804−6834.

(13) Sutherland, B. R.; Sargent, E. H. Perovskite Photonic Sources. *Nat. Photonics* **2016**, *10*, 295−302.

(14) Tan, Z. K.; Moghaddam, R. S.; Lai, M. L.; Docampo, P.; Higler, R.; Deschler, F.; Price, M.; Sadhanala, A.; Pazos, L. M.; Credgington, D.; Hanusch, F.; Bein, T.; Snaith, H. J.; Friend, R. H. Bright Light-emitting Diodes Based on Organometal Halide Perovskite. *Nat. Nanotechnol.* **2014**, *9*, 687−692.

DOI: 10.1021/acsphotonics.7b00520
ACS Photonics 2017, 4, 2281−2289

(15) Cho, H.; Jeong, S. H.; Park, M. H.; Kim, Y. H.; Wolf, C.; Lee, C. L.; Heo, J. H.; Sadhanala, A.; Myoung, N.; Yoo, S. Overcoming the Electroluminescence Efficiency Limitations of Perovskite Light-Emitting Diodes. *Science* **2015**, *350*, 1222−1225.
(16) Pan, J.; Sarmah, S. P.; Murali, B.; Dursun, I.; Peng, W.; Parida, M. R.; Liu, J.; Sinatra, L.; Alyami, N.; Zhao, C. Air-stable Surface-passivated Perovskite Quantum Dots for Ultra-robust, Single-and Two-photon-induced Amplified Spontaneous Emission. *J. Phys. Chem. Lett.* **2015**, *6*, 5027−5033.
(17) Stranks, S. D.; Wood, S. M.; Wojciechowski, K.; Deschler, F.; Saliba, M.; Khandelwal, H.; Patel, J. B.; Elston, S. J.; Herz, L. M.; Johnston, M. B. Enhanced Amplified Spontaneous Emission in Perovskites Using a Flexible Cholesteric Liquid Crystal Reflector. *Nano Lett.* **2015**, *15*, 4935−4941.
(18) Yakunin, S.; Protesescu, L.; Krieg, F.; Bodnarchuk, M. I.; Nedelcu, G.; Humer, M.; De Luca, G.; Fiebig, M.; Heiss, W.; Kovalenko, M. V. Low-threshold Amplified Spontaneous Emission and Lasing from Colloidal Nanocrystals of Caesium Lead Halide Perovskites. *Nat. Commun.* **2015**, *6*, 8056.
(19) Jia, Y.; Kerner, R. A.; Grede, A. J.; Brigeman, A. N.; Rand, B. P.; Giebink, N. C. Diode-pumped Organo-Lead Halide Perovskite Lasing in a Metal-clad Distributed Feedback Resonator. *Nano Lett.* **2016**, *16*, 4624−4629.
(20) Liu, X.; Ha, S. T.; Zhang, Q.; de la Mata, M.; Magen, C.; Arbiol, J.; Sum, T. C.; Xiong, Q. Whispering Gallery Mode Lasing from Hexagonal Shaped Layered Lead Iodide Crystals. *ACS Nano* **2015**, *9*, 687−695.
(21) Saliba, M.; Wood, S. M.; Patel, J. B.; Nayak, P. K.; Huang, J.; Alexander-Webber, J. A.; Wenger, B.; Stranks, S. D.; Hörantner, M. T.; Wang, J. T. W.; Nicholas, R. J.; Herz, L. M.; Johnston, M. B.; Morris, S. M.; Snaith, H. J.; Riede, M. K. Structured Organic−inorganic Perovskite Toward a Distributed Feedback Laser. *Adv. Mater.* **2016**, *28*, 923−929.
(22) Xing, G.; Mathews, N.; Lim, S. S.; Yantara, N.; Liu, X.; Sabba, D.; Grätzel, M.; Mhaisalkar, S.; Sum, T. C. Low-temperature Solution-processed Wavelength-tunable Perovskites for Lasing. *Nat. Mater.* **2014**, *13*, 476−480.
(23) Deschler, F.; Price, M.; Pathak, S.; Klintberg, L. E.; Jarausch, D. D.; Higler, R.; Hüttner, S.; Leijtens, T.; Stranks, S. D.; Snaith, H. J.; Atatüre, M.; Phillips, R. T.; Friend, R. H. High Photoluminescence Efficiency and Optically Pumped Lasing in Solution-Processed Mixed Halide Perovskite Semiconductors. *J. Phys. Chem. Lett.* **2014**, *5*, 1421−1426.
(24) Shi, Z. F.; Sun, X. G.; Wu, D.; Xu, T. T.; Tian, Y. T.; Zhang, Y. T.; Li, X. J.; Du, G. T. Near-infrared Random Lasing Realized in a Perovskite $CH_3NH_3PbI_3$ thin film. *J. Mater. Chem. C* **2016**, *4*, 8373−8379.
(25) Zhu, H.; Fu, Y.; Meng, F.; Wu, X.; Gong, Z.; Ding, Q.; Gustafsson, M. V.; Trinh, M. T.; Jin, S.; Zhu, X. Lead Halide Perovskite Nanowire Lasers with Low Lasing Thresholds and High Quality Factors. *Nat. Mater.* **2015**, *14*, 636−642.
(26) Niu, G.; Guo, X.; Wang, L. Review of Recent Progress in Chemical Stability of Perovskite Solar Cells. *J. Mater. Chem. A* **2015**, *3*, 8970−8980.
(27) Rong, Y.; Liu, L.; Mei, A.; Li, X.; Han, H. Beyond Efficiency: The Challenge of Stability in Mesoscopic Perovskite Solar Cells. *Adv. Energy Mater.* **2015**, *5*, 1501066.
(28) Yang, Z.; Rajagopal, A.; Jo, S. B.; Chueh, C. C.; Williams, S.; Huang, C. C.; Katahara, J. K.; Hillhouse, H. W.; Jen, A. K.-Y. Stabilized Wide Bandgap Perovskite Solar Cells by Tin Substitution. *Nano Lett.* **2016**, *16*, 7739−7747.
(29) Sanehira, E. M.; Tremolet de Villers, B. J.; Schulz, P.; Reese, M. O.; Ferrere, S.; Zhu, K.; Lin, L. Y.; Berry, J. J.; Luther, J. M. Influence of Electrode Interfaces on the Stability of Perovskite Solar Cells: Reduced Degradation Using MoO_x/Al for Hole Collection. *ACS Energy Letters* **2016**, *1*, 38−45.
(30) Song, J.; Li, J.; Li, X.; Xu, L.; Dong, Y.; Zeng, H. Quantum Dot Light-Emitting Diodes Based on Inorganic Perovskite Cesium Lead Halides ($CsPbX_3$). *Adv. Mater.* **2015**, *27*, 7162−7167.
(31) Wang, Y.; Li, X.; Song, J.; Xiao, L.; Zeng, H.; Sun, H. All-Inorganic Colloidal Perovskite Quantum Dots: A New Class of Lasing Materials with Favorable Characteristics. *Adv. Mater.* **2015**, *27*, 7101−7108.
(32) Wei, Z.; Perumal, A.; Su, R.; Sushant, S.; Xing, J.; Zhang, Q.; Tan, S. T.; Demir, H. V.; Xiong, Q. Solution-processed Highly Bright and Durable Cesium Lead Halide Perovskite Light-Emitting Diodes. *Nanoscale* **2016**, *8*, 18021−18026.
(33) Zhang, X.; Lin, H.; Huang, H.; Reckmeier, C.; Zhang, Y.; Choy, W. C.; Rogach, A. L. Enhancing the Brightness of Cesium Lead Halide Perovskite Nanocrystal Based Green Light-Emitting Devices through the Interface Engineering with Perfluorinated Ionomer. *Nano Lett.* **2016**, *16*, 1415−1420.
(34) Ling, Y.; Tian, Y.; Wang, X.; Wang, J. C.; Knox, J. M.; Perez-Orive, F.; Du, Y.; Tan, L.; Hanson, K.; Ma, B. Enhanced Optical and Electrical Properties of Polymer-Assisted All-Inorganic Perovskites for Light-Emitting Diodes. *Adv. Mater.* **2016**, *28*, 8983−8989.
(35) Eaton, S. W.; Lai, M.; Gibson, N. A.; Wong, A. B.; Dou, L.; Ma, J.; Wang, L. W.; Leone, S. R.; Yang, P. Lasing in Robust Cesium Lead Halide Perovskite Nanowires. *Proc. Natl. Acad. Sci. U. S. A.* **2016**, *113*, 1993−1998.
(36) Alivisatos, A. P. Semiconductor Clusters, Nanocrystals, and Quantum Dots. *Science* **1996**, *271*, 933−937.
(37) Klimov, V. I.; Mikhailovsky, A. A.; Xu, S.; Malko, A.; Hollingsworth, J. A.; Leatherdale, C. A.; Eisler, H. J.; Bawendi, M. G. Optical Gain and Stimulated Emission in Nanocrystal Quantum Dots. *Science* **2000**, *290*, 314−317.
(38) Wang, Y.; Li, X.; Zhao, X.; Xiao, L.; Zeng, H.; Sun, H. Nonlinear Absorption and Low-threshold Multiphoton Pumped Stimulated Emission from All-inorganic Perovskite Nanocrystals. *Nano Lett.* **2016**, *16*, 448−453.
(39) Xu, Y.; Chen, Q.; Zhang, C.; Wang, R.; Wu, H.; Zhang, X.; Xing, G.; Yu, W. W.; Wang, X.; Zhang, Y. Two-photon-pumped Perovskite Semiconductor Nanocrystal Lasers. *J. Am. Chem. Soc.* **2016**, *138*, 3761−3768.
(40) Wang, Y.; Li, X.; Nalla, V.; Zeng, H.; Sun, H. Solution-Processed Low Threshold Vertical Cavity Surface Emitting Lasers from All-Inorganic Perovskite Nanocrystals. *Adv. Funct. Mater.* **2017**, *27*, 1605088.
(41) Chang-Hasnain, C. J. Tunable VCSEL. *IEEE J. Sel. Top. Quantum Electron.* **2000**, *6*, 978−987.
(42) Lidzey, D. G.; Bradley, D.; Skolnick, M.; Virgili, T.; Walker, S.; Whittaker, D. Strong Exciton−Photon Coupling in an Organic Semiconductor Microcavity. *Nature* **1998**, *395*, 53−55.
(43) Tessler, N.; Denton, G. J.; Friend, R. H. Lasing from Conjugated-Polymer Microcavities. *Nature* **1996**, *382*, 695.
(44) Dang, C.; Lee, J.; Breen, C.; Steckel, J. S.; Coe-Sullivan, S.; Nurmikko, A. Red, Green and Blue Lasing Enabled by Single-Exciton Gain in Colloidal Quantum Dot Films. *Nat. Nanotechnol.* **2012**, *7*, 335−339.
(45) Weng, G.; Mei, Y.; Liu, J.; Hofmann, W.; Ying, L.; Zhang, J.; Bu, Y.; Li, Z.; Yang, H.; Zhang, B. Low Threshold Continuous-Wave Lasing of Yellow-Green InGaN-QD Vertical-Cavity Surface-Emitting Lasers. *Opt. Express* **2016**, *24*, 15546−15553.
(46) Yassitepe, E.; Yang, Z.; Voznyy, O.; Kim, Y.; Walters, G.; Castañeda, J. A.; Kanjanaboos, P.; Yuan, M.; Gong, X.; Fan, F.; Pan, J.; Hoogland, S.; Comin, R.; Bakr, O. M.; Padilha, L. A.; Nogueira, A. F.; Sargent, E. H. Amine-Free Synthesis of Cesium Lead Halide Perovskite Quantum Dots for Efficient Light-Emitting Diodes. *Adv. Funct. Mater.* **2016**, *26*, 8757−8763.
(47) Chen, S.; Zhang, C.; Lee, J.; Han, J.; Nurmikko, A. High-Q, Low-Threshold Monolithic Perovskite Thin-Film Vertical-Cavity Lasers. *Adv. Mater.* **2017**, *29*, 1604781.
(48) Boles, M. A.; Ling, D.; Hyeon, T.; Talapin, D. V. The Surface Science of Nanocrystals. *Nat. Mater.* **2016**, *15*, 141−153.
(49) Cadelano, M.; Sarritzu, V.; Sestu, N.; Marongiu, D.; Chen, F.; Piras, R.; Corpino, R.; Carbonaro, C. M.; Quochi, F.; Saba, M. Can Trihalide Lead Perovskites Support Continuous Wave Lasing? *Adv. Opt. Mater.* **2015**, *3*, 1557−1564.
(50) Milot, R. L.; Eperon, G. E.; Snaith, H. J.; Johnston, M. B.; Herz, L. M. Temperature-Dependent Charge-Carrier Dynamics in $CH_3NH_3PbI_3$ Perovskite Thin Films. *Adv. Funct. Mater.* **2015**, *25*, 6218−6227.

DOI: 10.1021/acsphotonics.7b00520
ACS Photonics 2017, 4, 2281−2289

(51) Chen, S.; Roh, K.; Lee, J.; Chong, W. K.; Lu, Y.; Mathews, N.; Sum, T. C.; Nurmikko, A. A Photonic Crystal Laser from Solution Based Organo-lead Iodide Perovskite Thin Films. *ACS Nano* **2016**, *10*, 3959−3967.
(52) Fu, Y.; Zhu, H.; Schrader, A. W.; Liang, D.; Ding, Q.; Joshi, P.; Hwang, L.; Zhu, X. Y.; Jin, S. Nanowire Lasers of Formamidinium Lead Halide Perovskites and Their Stabilized Alloys with Improved Stability. *Nano Lett.* **2016**, *16*, 1000−1008.
(53) Li, J.; Xu, L.; Wang, T.; Song, J.; Chen, J.; Xue, J.; Dong, Y.; Cai, B.; Shan, Q.; Han, B.; Zeng, H. 50-Fold EQE Improvement up to 6.27% of Solution-Processed All-Inorganic Perovskite $CsPbBr_3$ QLEDs via Surface Ligand Density Control. *Adv. Mater.* **2017**, *29*, 1603885.
(54) Chiba, T.; Hoshi, K.; Pu, Y. J.; Takeda, Y.; Hayashi, Y.; Ohisa, S.; Kawata, S.; Kido, J. High-Efficiency Perovskite Quantum-Dot Light-Emitting Devices by Effective Washing Process and Interfacial Energy Level Alignment. *ACS Appl. Mater. Interfaces* **2017**, *9*, 18054−18060.
(55) Whitworth, G. L.; Harwell, J. R.; Miller, D. N.; Hedley, G. J.; Zhang, W.; Snaith, H. J.; Turnbull, G. A.; Samuel, I. D. Nanoimprinted Distributed Feedback Lasers of Solution Processed Hybrid Perovskites. *Opt. Express* **2016**, *24*, 23677−23684.
(56) Cha, H.; Bae, S.; Lee, M.; Jeon, H. Two-dimensional Photonic Crystal Bandedge Laser with Hybrid Perovskite Thin Film for Optical Gain. *Appl. Phys. Lett.* **2016**, *108*, 181104.
(57) Pourdavoud, N.; Wang, S.; Mayer, A.; Hu, T.; Chen, Y.; Marianovich, A.; Kowalsky, W.; Heiderhoff, R.; Scheer, H. C.; Riedl, T. Photonic Nanostructures Patterned by Thermal Nanoimprint Directly into Organo-Metal Halide Perovskites. *Adv. Mater.* **2017**, *29*, 1605003.
(58) Fu, Y.; Zhu, H.; Stoumpos, C. C.; Ding, Q.; Wang, J.; Kanatzidis, M. G.; Zhu, X.; Jin, S. Broad Wavelength Tunable Robust Lasing from Single-crystal Nanowires of Cesium Lead Halide Perovskites ($CsPbX_3$, X= Cl, Br, I). *ACS Nano* **2016**, *10*, 7963−7972.
(59) He, X.; Liu, P.; Zhang, H.; Liao, Q.; Yao, J.; Fu, H. Patterning Multicolored Microdisk Laser Arrays of Cesium Lead Halide Perovskite. *Adv. Mater.* **2017**, *29*, 1604510.

DOI: 10.1021/acsphotonics.7b00520
ACS Photonics 2017, 4, 2281−2289